For submission to *Environmental Technology* as a Research Article

# Tracing morphological characteristics of activated sludge flocs by using a digital microscope and their effects on sludge dewatering and settling

*Yuki Nakaya*, Jinming Jia*, Hisashi Satoh**^

*Division of Environmental Engineering, Faculty of Engineering, Hokkaido University, North-13, West-8, Sapporo 060-8628, Japan.

^Corresponding author

ORCID:

Yuki Nakaya: 0000-0003-4068-5772

Hisashi Satoh: 0000-0002-5222-9689

**Abstract**

In wastewater treatment by the activated sludge (AS) process, settleability and dewaterability of AS are key issues that are directly related to the treated water quality and sludge treatment costs. Several studies investigated the relationship between the shape of AS flocs and their settling/dewatering property. To quantify the floc morphology, it is imperative to attach a camera to a microscope or move the stage manually. Hence, labor and equipment costs may increase. In this study, by combining a digital microscope and an automatic stage, more than

100 magnified floc images were rapidly obtained from one AS sample dropped on a slide glass, and shape parameters were collectively calculated using an analysis software. During 1-year monitoring of four wastewater treatment plants in Sapporo City (Hokkaido, Japan), the morphological parameters and extracellular polymeric substances (EPS) quantity/quality of AS were analyzed on the basis of their correlation to the time to filtration (TTF) and sludge volume index (SVI), which are indicators for describing the settling and dewatering properties of AS, respectively. In one plant, larger, denser, and smoother flocs tended to contain less EPS and exhibited better sludge dewaterability. In another plant, larger, denser, and smoother flocs were considered to contribute to better settlement. Especially, an equivalent high-density floc diameter and the ratio of mixed liquor suspended solids (MLSS) concentration to the total floc area were commonly suggested to explain AS settleability and dewaterability.

**Keywords**

Activated sludge; Extracellular polymeric substances; Microscopic image; Sludge volume index; Time to filtration.

## 1. Introduction

Generally, municipal and industrial wastewater treatment plants (WWTPs) are subjected to biological treatment, in which pollutants such as chemical oxygen demand (COD), phosphorus, and nitrogen are degraded or removed by microbial activity [1]. After the completion of biological treatment, it is crucial to separate the biomass [activated sludge (AS)] from the supernatant to obtain a clear effluent. Often, the separation of AS from the liquid phase includes two steps. First, AS is separated from the liquid phase by gravity settling in a clarifier. The worse sludge settleability would cause a turbid effluent and biomass washout [2], thereby affecting treatment performance. The sludge volume index (SVI) is mainly used as an indicator for sludge settleability. If the SVI is high, the sludge settleability will worsen, and the risk of biomass washout will be high. Second, the excess AS can be further dewatered for final disposal or additional treatment. Worse dewaterability would increase the total treatment costs; excess AS treatment contributes almost half to the wastewater treatment cost [3], even though worse dewaterability may not affect the effluent water quality. To evaluate dewaterability, time to filtration (TTF), specific resistance to filtration (SRF), and capillary suction time (CST) are generally considered. Under the same measurement conditions, high values of TTF, SRF, or CST suggest the worse sludge filterability and dewaterability.

Poor AS settling, referred to as bulking, is mainly classified as filamentous bulking and viscous bulking based on floc characteristics [4]. Filamentous bulking is actually related to the overgrowth of protruding filamentous bacteria in AS. In contrast, viscous bulking is primarily caused by the proliferation of *Zoogloea* sp. in AS. The *Zoogloea* sp. lose their flagella under a food-limited condition, leading to the accumulation of waste products outside the cell wall. The products form a thick and sticky slime layer, thereby reducing the sludge density and eventually hindering sludge settling.

In addition to the effects of bacteria, extracellular polymeric substances (EPSs), which are mainly high-molecular-weight metabolic products from the microorganisms of AS, can be potentially responsible for the worse AS settleability or dewaterability [5]. For settleability, contradictory theories have been suggested in previous studies. In the winter season or under low-temperature conditions, the content of EPSs that can be extracted from AS is greater than that extracted under other conditions, coinciding with a higher SVI [6,7]. However, a negative correlation between the total EPS and the SVI was observed in some studies: The concentration of EPSs, especially hydrophobic protein EPSs, was reported to decrease with the increase in the SVI [8]. On the other hand, a complex correlation between EPS and SRF was reported, and this correlation varied in different studies. Peng et al. conducted statistical analysis and suggested that SVI, CST, and SRF values were not associated with physicochemical properties [9]. However, the ratio of carbohydrate EPS and protein EPS exhibited a positive correlation with SRF in their study [9]. Meanwhile, Cetin et al. reported that the filterability and compactibility of sludge samples were considerably improved with the increase in the carbohydrate content and decrease in the protein content of the sludge EPS [10]. Other studies suggested that EPSs exhibited a positive correlation to SRF [11,12]. However, EPS evaluation requires the selection of an appropriate extraction procedure from various methods [5], analysis equipment, and labor costs and time consumption. This may make it difficult to easily implement sludge diagnosis by EPS analysis in real treatment plants.

On the other hand, analysis of visual information such as the color and shape of sludge has been considered as a simpler method of sludge diagnosis [13]. In particular, the following studies have been conducted on the relationship between sludge morphology, sludge settleability, and dewaterability using a microscope. For example, the fractal dimension (FD) of AS flocs has been employed to describe the geometric features of AS flocs in previous studies [14–18]. In fractal theory, the FD is determined by the perimeter–area relationship based on image analysis [14], and it is quantified by a value from 1 to 3 [19]. Thus, it is a key parameter that is commonly employed to quantitatively describe the heterogeneous structure associated with the density, strength, and compactness of AS flocs [20]. The fractal structure of AS flocs is widely known to considerably impact the efficiency of wastewater treatment [19]. For example, FD obtained from the AS floc image has become a tool to evaluate the bioactivity and settleability of AS [18]. The weak floc structure and small floc size, which are morphological feature of AS, are also crucial in the dewatering process [3,15].

Even though the floc morphology can provide additional information regarding the properties of AS and serve as an indicator for the worse sludge settling or dewatering condition, the time consumption and high costs required for manual microscopic observations can make routine monitoring difficult, as was pointed out in the previous research [13]. To reduce costs, a digital microscope camera can be applied for image acquisition. Previously, images captured by our group using a tabletop digital microscope were trained by a convolutional neural network (CNN)-based deep-learning program (inception-V3 model) for the identification of sludge bulking, a training accuracy of ~95% was achieved, and a 20% morphological change was recognized [21].

Based on the successful introduction of the digital microscope, in this study, images recorded using the digital microscope were used for the quantification of the shape characteristics of AS. To the best of our knowledge, no previous study has combined a digital microscope with an automated stage to obtain morphological parameters of AS and used them to follow the gradual changes in settling and dewatering of sludge over a one-year period. The objective was to apply cost-effective, quantified image analysis to provide morphological insights into the AS settling and dewatering difficulties, which combined EPS analysis as a contrast. Then, seasonal variations in settling and dewatering conditions of different WWTPs were monitored, and the key contributors to the worse dewaterability and settleability were discussed.

## 2. Materials and Methods

### *2.1. Sources of activated sludge samples*

AS samples were collected near the outlet of the final stage aeration tank of four full-scale wastewater treatment plants (WWTPs) located in Sapporo City, Japan [22] from July 2020 to June 2021. These WWTPs were mainly used for the treatment of domestic wastewater. Table S1 summarizes the operating conditions of these WWTPs and the physicochemical water quality after treatment. Fig. S1 shows the hydraulic load per day and influent water temperature of these WWTPs during the study period. WWTP-A, B, and C are connected to a combined sewer system. Thus, the influent water volume was sometimes large due to sudden precipitation. However, WWTP-D is connected only to a separate sewer system. Hence there was not much increase in the influent water volume. In all WWTPs, the hydraulic load increased in March and April due to the generation of snowmelt water. In addition, the influent water temperature at WWTP-D was relatively higher than that at other plants because it received wastewater from a sludge treatment facility attached to the WWTP-D. A 1.5-L AS sample from each WWTP was collected in a 2-L polypropylene bottle and transferred to our laboratory at 4 °C with neither feeding nor aeration. The collected samples were analyzed within 1 h after sampling.

*2.2. Analytical methods*

*2.2.1 Determination of sludge dewaterability and settleability*

AS dewaterability was determined by the filterability test [11,23]. *TTF* and *SRF* were evaluated on the basis of the method. In brief, dead-end filtration tests were conducted using a vacuum filtration setup. A Buchner funnel with a glass-fiber filter paper (GS-25; ADVANTEC, Tokyo, Japan) having a pore size of 0.6 μm was used to filter 50 mL of the AS sample, and a constant vacuum pressure of 0.05 MPa was applied by a vacuum pump (MAD-015A; ULVAC, Kanagawa, Japan). A graduated cylinder was set under the funnel. The time required for the filtration of 13, 15, 17, 20, 25, 30, and 35 mL of the AS sample was recorded using a stopwatch. Then, the final time to filter 50 mL of the sample was recorded and defined as *TTF*. The measurements were conducted in triplicate, and average values were taken. The measurements were performed using samples collected between February 2021 and June 2021.

*SVI* was calculated by Eq. 1 [23]:

$$SVI\ (mL/g) = \frac{V \times 1000}{MLSS} \qquad \text{Eq. 1}$$

where *V* is the volume of the settled AS in a 1 L cylinder after 30 min (mL/L), 1000 is a conversion factor (mg/g), and *MLSS* is the mixed liquor suspended solids (MLSS) (mg/L). MLSS was measured according to a standard method [23]. SVI measurements were performed using samples collected between July 2020 and June 2021.

*2.2.2 Extraction and analysis of EPS*

In the AS mixed liquor, some EPSs exist outside the AS flocs, which are called soluble EPSs. On the other hand, some other EPSs exist inside the floc structure, which are called bound EPSs. The bound EPSs can be further subdivided into loosely bound (LB) EPSs and tightly bound (TB) EPSs. In this study, LB and TB EPSs were extracted according to the heating extraction method modified by Li and Yang [11]. First, 25 mL of a well-mixed AS sample was allowed to settle down at 4,000×*g* for 15 min in a 40-mL centrifuge tube, and the supernatant was discarded. The pellets were resuspended in their original volume with a 0.05% NaCl solution at 70 °C, and then the suspension was mixed well in a vortex mixer for 1 min. The suspension was centrifuged at 4,000×*g* for 15 min, and the supernatant and pellet were collected separately. The organic matter in the supernatant was regarded as the LB EPS of the biomass.

Second, for the extraction of the TB EPS, the obtained pellet was resuspended in its original volume of a 0.05% NaCl solution at 60 °C, mixed in a vortex mixer for 1 min, and incubated in a water bath at 60 °C for 30 min. The extracted solution was obtained by centrifugation at 4,000×*g* for 15 min. The organic matter in the supernatant was regarded as the TB EPS of the biomass. Then, the dry weight of extracted activated sludge was measured by drying the settled sludge pellet (SSP) in a dryer (FS-405, ADVANTEC, Tokyo, Japan) at 105 °C for more than 3 hours, measuring the weight using a balance at room temperature, and subtracting the previously measured weight of the tube.

All chemical analyses of EPS were conducted in triplicate using analytical-grade chemicals. Proteins and carbohydrates in the extracted LB(TB) EPS were quantified according to the procedure reported by Frølund et al. [24]. The protein content was determined by the DC protein assay (BIO-RAD, California, USA) based on the Lowry method using bovine serum albumin (BSA) as the standard. The carbohydrate (polysaccharide) content was measured by the anthrone-sulfuric acid method using glucose as the standard. As these EPS contents were originally derived from the sludge pellet in the first procedure, the protein and carbohydrate contents of the extracted LB(TB) EPS were defined as amounts per unit dry sludge weight [*PN-LB(TB)-EPS* (mg/g-SSP) and *CH-LB(TB)-EPS* (mg/g-SSP), respectively]. Finally, the sum of *PN(CH)-LB-EPS* and *PN(CH)-TB-EPS* was regarded as the total amount of protein (carbohydrate) EPS [*PN(CH)-EPS* (mg/g-SSP)]. The sum of *PN-EPS* and *CH-EPS* was regarded as the total amount of EPS [*Total-EPS* (mg/g-SSP)]. In addition, the ratio between *PN-EPS* and *CH-EPS* (*PN/CH*) was calculated.

*2.2.3 Image analysis*

Morphological properties of AS were evaluated by microscopic image analysis. Floc images were recorded using a tabletop digital microscope (UM06; Kenis Ltd., Osaka, Japan), which was coupled with a 10× objective lens and a high-precision motorized XY stage (mmu-60×; Chuo Precision Industrial Co., Ltd., Tokyo, Japan) [21]; this XY stage controlled the movement of a sample slide without the overlap of images. A 50-µL droplet of AS was set on a slide. Then, the sample was covered carefully with a cover slide (18 × 18 mm). The slide was illuminated by a white LED light from a smartphone from the back. By the automatic control of the stage and photographing function, 154 images were photographed from one slide. One photograph covered an area of 1.05 mm by 1.40 mm. In the original floc images, the AS flocs generally exhibited a deeper color than the brighter background.

The images were subsequently processed using Image-Pro Plus 6.0 (Media Cybernetics, Inc., Maryland, USA). First, small debris and filamentous bacteria were discriminated from AS flocs as follows. Filtration using a close filter with a 2 × 2 kernel was repeated twice. This process fills gaps of dark objects and connects nearby bright objects via the magnification of bright areas (protrusions) that penetrate the dark objects. Therefore, the colors of filamentous bacteria and weak flocs, which are small with an elongated shape, are processed to be similar to the bright background. Finally, by using a built-in color-histogram-based edge detection algorithm, the filamentous bacteria and weak flocs were not recognized as dark objects, and only a core area of AS with a dark color was recognized as presenting objects, which were named as high-density flocs (Fig. 1).

Second, to recognize all of the floc areas in the original image by using the color-histogram-based edge detection algorithm, an erode filter with 2 × 2 kernel and a median filter were applied. The former erodes edges of bright objects and magnifies dark ones. The erode filter was used twice. Then, the median filter, which replaces a center pixel with the median value of the surrounding pixels, was applied to blur the image. After processing these two filters, all floc areas were recognized by the algorithm, and the objects were referred to as the total flocs (Fig. 1).

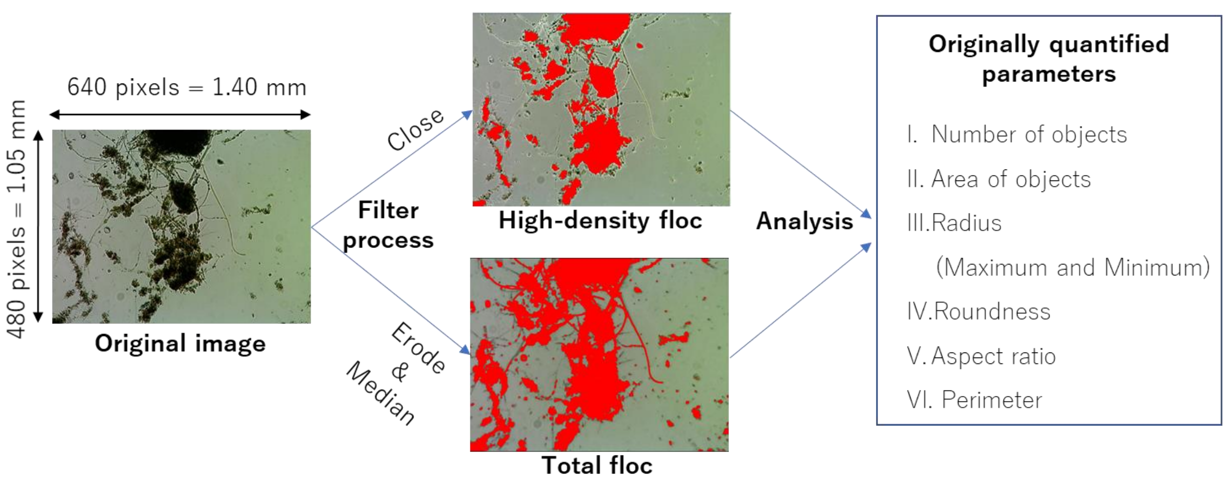


**Fig. 1.** Schematic of the image processing protocols.

Thereafter, morphological data of the high-density flocs and the total flocs were calculated from all of the 154 images using 50-μL AS, resulting in class-specific variables, i.e., floc area, perimeter, and the maximum/minimum radius of each floc (Fig. 1). Based on these variables, the following morphological parameters were calculated using each of the following mathematical equations:

(1) Area of filamentous bacteria and weak flocs ($A_{\mathrm{F\&Wfs}}$).

$$A_{\mathrm{F\&Wfs}}\ (mm^2/mL) = \frac{A_{\mathrm{T}}\ (mm^2) - A_{\mathrm{HD}}\ (mm^2)}{0.05\ (mL) \times 0.75} \qquad \text{Eq. 2}$$

Here, $A_{\mathrm{T}}$ is the sum of areas of the total flocs, $A_{\mathrm{HD}}$ is the sum of areas of high-density flocs, and 0.75 is a factor corresponding to the ratio of the imaging range that can be photographed by the system to the area of the cover glass covering the AS.

(2) Ratio of MLSS to the total floc area ($MLSS/A_{\mathrm{T}}$) (μg/mm$^2$), which was used to evaluate the compactness of the AS flocs.

$$MLSS/A_{\mathrm{T}}\ \ (\mu g/mm^2) = \frac{MLSS\ (mg/L) \times 0.05\ (mL) \times 0.75}{A_{\mathrm{T}}(mm^2)} \qquad \text{Eq. 3}$$

(3) Fraction of the high-density flocs in the total floc area ($A_{\mathrm{HD}}/A_{\mathrm{T}}$), which was employed to evaluate the ratio of high-density flocs to the total AS flocs.

$$A_{HD}/A_T\ = \frac{A_{\mathrm{HD}}(mm^2)}{A_{\mathrm{T}}\ (mm^2)} \qquad \text{Eq. 4}$$

(4) The total EPS content of the unit floc area ($EPS/A_{\mathrm{T}}$), which was used to evaluate the EPS content of the unit floc area.

Eq. 5

$$EPS/A_T\ (ng\text{-}EPS/mm^2) = \frac{Total\text{-}EPS\ (mg/g\text{-}SSP) \times MLSS\ (mg/L) \times 0.05\ (mL) \times 0.75}{A_T\ (mm^2)}$$

(5) Aspect ratio (*AR*).

$$AR = \frac{4[Radius_{\max}(mm) - Radius_{\min}(mm)]}{\pi \times Radius_{\min}(mm)} + 1 \quad \text{Eq. 6}$$

This followed the definition adopted in previous studies [25,26] as the three-dimensional aspect ratio. Here, $Radius_{\max}$ and $Radius_{\min}$ (maximum and minimum radius) were obtained for each of the "total flocs" of interest. The final *AR* for one AS sample droplet was determined from the average *AR* values of the recognized flocs. The AR describes the elongation of an object. The AR of one circular particle should be 1, and it would be higher when the object becomes more elongated and irregular.

(6) Roundness (*RN*).

$$RN = \frac{Perimeter^2\ (mm^2)}{4\pi \times Area\ of\ the\ total\ flocs(mm^2)} \quad \text{Eq. 7}$$

Here, *Perimeter* and *Area of the total flocs* (not $A_T$) were obtained for each of the "total flocs" of interest. The roundness of a floc was calculated by a software built-in algorithm. The final *RN* for each AS droplet was determined by average *RN* values of the recognized flocs. Roundness describes the shape of one object. The roundness of a circular object is 1, while that of the other shapes is greater than 1. Although the authors recognize that the general definition of roundness is the inverse of the definition of roundness in this study (Eq. 7), the default calculation in the image analysis software was employed in this study.

(7) Fractal dimension (*FD*)

Based on the fractal theory, the area and perimeter of a two-dimensional object indicates correlation according to the following expression.

$$Area\ of\ the\ total\ flocs \propto Perimeter^{FD} \qquad \text{Eq. 8}$$

FD describes the boundary of an object, and the *FD* value of a two-dimensional object ranges from 1 to 2. It is generally higher when an AS floc exhibits a smooth and regular boundary as well as a compact shape [18]. In our study, the *FD* of each AS droplet was obtained from the slope of the double logarithmic plot for the *Area of the total flocs* and *Perimeter of the total flocs*.

(8) Equivalent high-density floc diameter ($D_{\mathrm{eqHD}}$) and equivalent total floc diameter ($D_{\mathrm{eqT}}$)

$$D_{\mathrm{eqHD}}(mm) = 2\sqrt{\frac{Area\ of\ the\ high\ density\ flocs\ (mm^2)}{\pi}} \qquad \text{Eq. 9}$$

$$D_{\mathrm{eqT}}(mm) = 2\sqrt{\frac{Area\ of\ the\ total\ flocs\ (mm^2)}{\pi}} \qquad \text{Eq. 10}$$

The equivalent high-density floc diameter was obtained for each of the high-density flocs of interest as the size of a high-density part of the floc or particle. The equivalent total floc diameter was obtained for each of the total flocs of interest as the size of the entire floc including filamentous bacteria and weak flocs. The final values for each AS droplet were determined by the average values of the recognized flocs; the increase in the number of small objects results in the decrease of $D_{\mathrm{eqHD}}$ and $D_{\mathrm{eqT}}$. These two floc size parameters were used to evaluate the size distribution of fine particles and flocs.

Finally, 11 parameters (Table 1) were obtained from one AS droplet. They were correlated with *TTF* and *SVI* to determine the cause for the deterioration of the AS dewaterability and settleability, respectively.

**Table 1.** Parameters of interest for correlation to sludge dewaterability and settleability.

| **Classification** | **Parameter** | | | |
|---|---|---|---|---|
| **Chemical** | *Total-EPS* | *PN/CH* | | |
| **Density** | $MLSS/A_{\mathrm{T}}$ | $A_{\mathrm{HD}}/A_{\mathrm{T}}$ | $EPS/A_{\mathrm{T}}$ | |
| **Morphology** | $A_{\mathrm{F\&Wfs}}$ | *FD* | *RN* | *AR* |
| **Size** | $D_{\mathrm{eqHD}}$ | $D_{\mathrm{eqT}}$ | | |

## 3. Results

### *3.1. Dewaterability and characteristics of activated sludge*

Fig. 2 shows the *TTF* of the four WWTPs. The TTF of WWTP-C was the highest throughout the experimental period. It increased from 360 s on February 18th to 850 s on April 2nd, and it decreased to 260 s on April 21st. The TTF values of WWTP-B was slightly greater than those of WWTP-A and WWTP-D in March and April. It decreased to the same level as those for WWTP-A and WWTP-D in May.

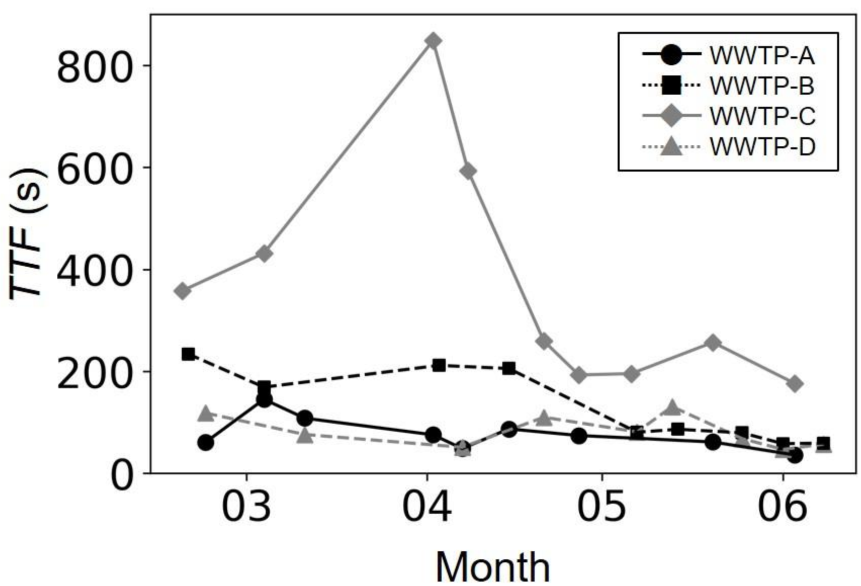

**Fig. 2.** Changes in the *TTF* for the four WWTPs during the experimental period between February 2021 and June 2021.

Table 2 summarizes all of the Pearson correlation coefficients calculated for *TTF* (or *SRF*) and the 11 parameters. Since the seasonal variation of *TTF* of WWTP-A, B, and D was small, the authors decided to focus on the correlation between *TTF* and shape parameters of WWTP-C, where relatively large seasonal variation was observed. Among the significant parameters investigated (Table 1), six parameters were positively or negatively correlated to the TTF with relatively higher correlation coefficients (|correlation coefficient |＞0.50) (Table 2 and Fig. 3). The total EPS amount (*Total-EPS*) increased with the increase in the *TTF* in WWTP-C [Fig. 3(a)]. The decrease in the floc density ($MLSS/A_T$) and in the fraction of high-density AS flocs ($A_{HD}/A_T$) was correlated to the increase in *TTF* [Figs. 3(b) and (c)]. That is, with the increase in the fraction of the small flocs, *TTF* increased [Fig. 3(c)]. With the decrease in *FD*, *TTF* also increased, indicative of the decrease in floc smoothness [Fig. 3(d)]. A negative correlation between *TTF* and $D_{eqHD}$ [Fig. 3(e)] or $D_{eqT}$ [Fig. 3(f)] suggested that AS, which on average comprised large flocs, exhibited low dewaterability. These results implied that dense, large, and smooth flocs containing less EPS are beneficial to sludge dewaterability as for WWTP-C.

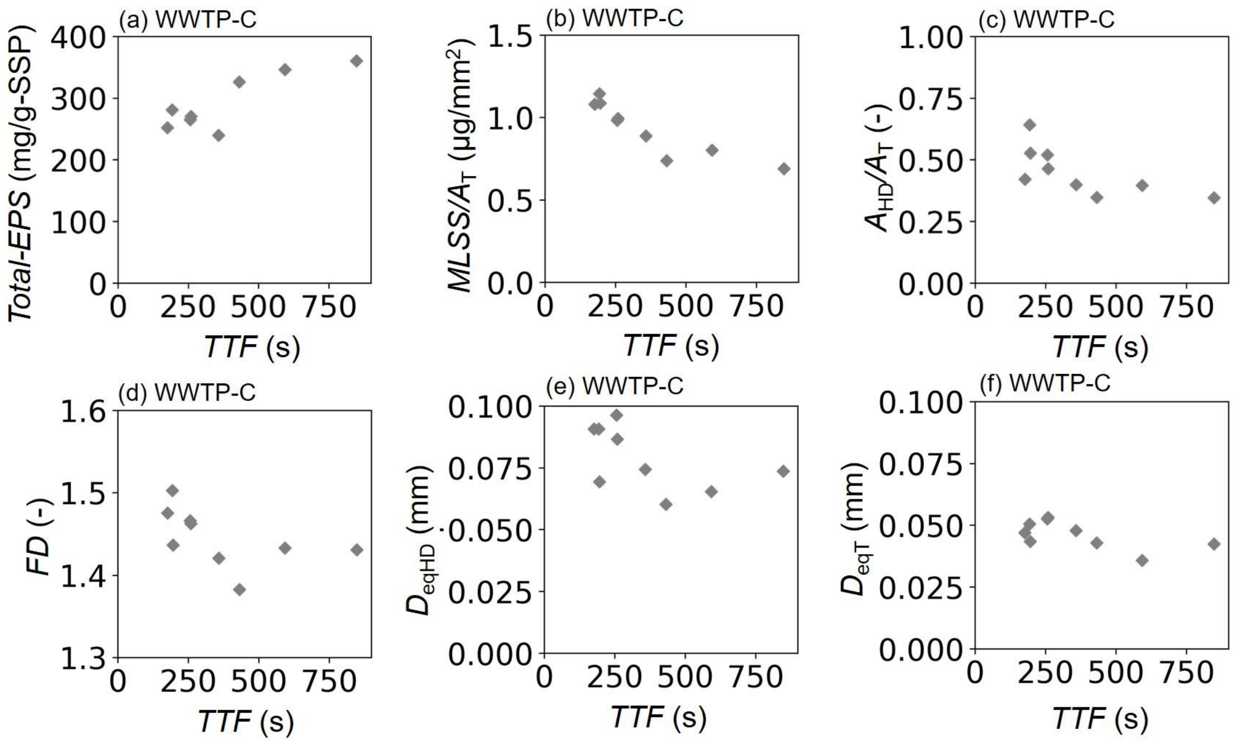


**Fig. 3.** Representative correlation diagrams between *TTF* and AS parameters of WWTP-C: (a) *TTF* versus the *Total-EPS*; (b) *TTF* versus the $MLSS/A_T$; (c) *TTF* versus the $A_{HD}/A_T$; (d) *TTF* versus the *FD*; (e) *TTF* versus the $D_{eqHD}$; (f) *TTF* versus the $D_{eqT}$.

**Table 2.** Pearson correlation coefficients calculated for *TTF*, *SVI* and the 11 parameters.

| | ***TTF*** | | | | ***SVI*** | | | |
|---|---|---|---|---|---|---|---|---|
| **WWTP-** | A | B | C | D | A | B | C | D |
| ***Total-EPS*** | 0.54 | 0.16 | 0.85 | 0.77 | 0.01 | 0.60 | −0.48 | 0.14 |
| ***PN/CH*** | −0.41 | 0.21 | 0.10 | 0.41 | −0.32 | 0.04 | 0.01 | −0.16 |
| $\boldsymbol{MLSS/A_{T}}$ | −0.48 | −0.30 | −0.89 | −0.27 | −0.55 | 0.02 | −0.25 | −0.49 |
| $\boldsymbol{A_{HD}/A_{T}}$ | −0.04 | −0.56 | −0.68 | −0.07 | −0.06 | 0.30 | −0.34 | −0.32 |
| $\boldsymbol{EPS/A_{T}}$ | 0.01 | −0.43 | −0.33 | −0.08 | −0.44 | 0.40 | −0.46 | −0.42 |
| $\boldsymbol{A_{F\&Wfs}}$ | 0.45 | 0.70 | 0.45 | 0.14 | 0.29 | −0.16 | 0.72 | 0.54 |
| ***FD*** | −0.48 | −0.38 | −0.51 | −0.32 | −0.09 | 0.25 | 0.01 | −0.49 |
| ***RN*** | −0.58 | 0.43 | −0.35 | −0.12 | 0.44 | 0.42 | 0.26 | 0.55 |
| ***AR*** | −0.30 | 0.30 | 0.36 | 0.05 | 0.39 | 0.39 | −0.19 | 0.37 |
| $\boldsymbol{D_{eqHD}}$ | 0.27 | −0.53 | −0.62 | 0.31 | −0.43 | 0.31 | −0.14 | −0.48 |
| $\boldsymbol{D_{eqT}}$ | −0.15 | −0.25 | −0.53 | −0.17 | 0.18 | 0.47 | 0.07 | 0.05 |

### *3.2. Settleability and characteristics of activated sludge*

Fig. 4 shows the *SVI* of the four WWTPs. The SVI of WWTP-A was less than 150 mL/g throughout the experimental period. Notably, an *SVI* of 150 mL/g is typically regarded as the threshold SVI for sludge bulking [4,27]. The SVI of WWTP-B was less than 160 mL/g except for January. The SVI values ranged from 160 mL/g to 220 mL/g in January, in which the inflow wastewater temperature was the lowest at 13°C in WWTP-B (Fig. S1). Generally, the SVI value of WWTP-C was greater than those of WWTP-A and WWTP-B, which was 200 mL/g on average and exhibited a peak on January14th (Fig. 4). The SVI of WWTP-D exhibited a seasonal variation. The SVI values were less than 130 mL/g between July and October 2020. These values increased in November, reaching the maximum on February 10, 2021 and decreased to 150 mL/g in May.

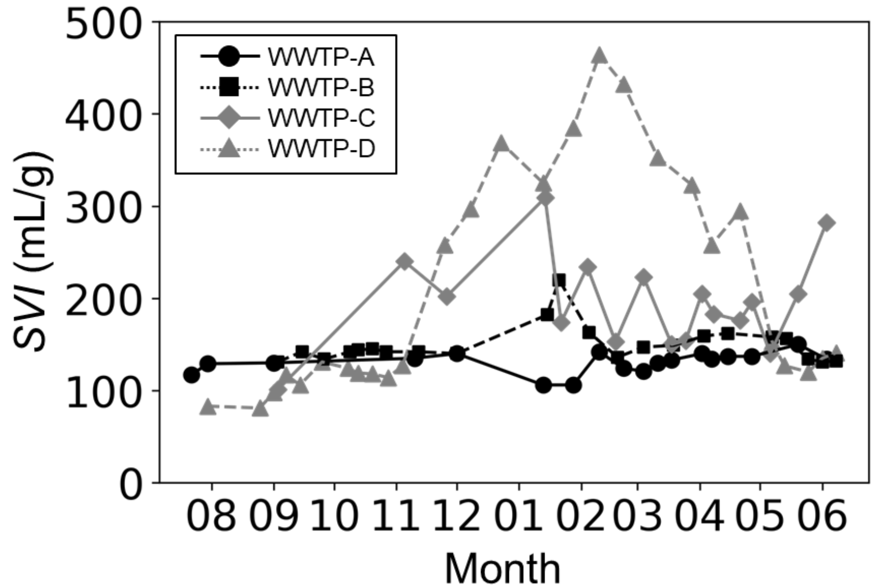


**Fig. 4.** Changes in the *SVI* of the four WWTPs during the experimental period between July 2020 and June 2021.

Table 2 also summarizes the Pearson correlation coefficients calculated for *SVI* and the 11 parameters. Here, the data of WWTP-C and D were further used to evaluate the contribution of the 11 characteristics of AS to the seasonal deterioration of settleability. There was a significant positive correlation between *SVI* and $A_{\mathrm{F\&Wfs}}$ (0.72 of the Pearson correlation coefficient) for the data of WWTP-C [Fig. 5(a)]. Although the seasonal variation of SVI was the largest in WWTP-D, only a few parameters were correlated to *SVI* of greater than 0.50 of the Pearson correlation coefficient (Table 2). Here, $MLSS/A_{\mathrm{T}}$, $A_{\mathrm{F\&Wfs}}$, *FD*, *RN*, and $D_{\mathrm{eqHD}}$ were discussed as parameters with relatively large correlation coefficients. The decrease in density ($MLSS/A_{\mathrm{T}}$) was considered to be related to the increase in *SVI* [Fig. 5(b)]. A positive correlation was obtained between *SVI* and $A_{\mathrm{F\&Wfs}}$ as well as in the case of WWTP-C [Fig. 5(c)]. *SVI* increased with decreasing *FD*, i. e., with decreasing surface smoothness of floc [Fig. 5(d)]. *SVI* and *RN* were positively correlated

[Fig. 6(e)]. With the increase in the fraction of the small flocs (namely $D_{eqHD}$ decreased), *SVI* increased [Fig. 6(f)]. These results implied that dense, large, and smooth flocs are beneficial to sludge settleability as for WWTP-D.

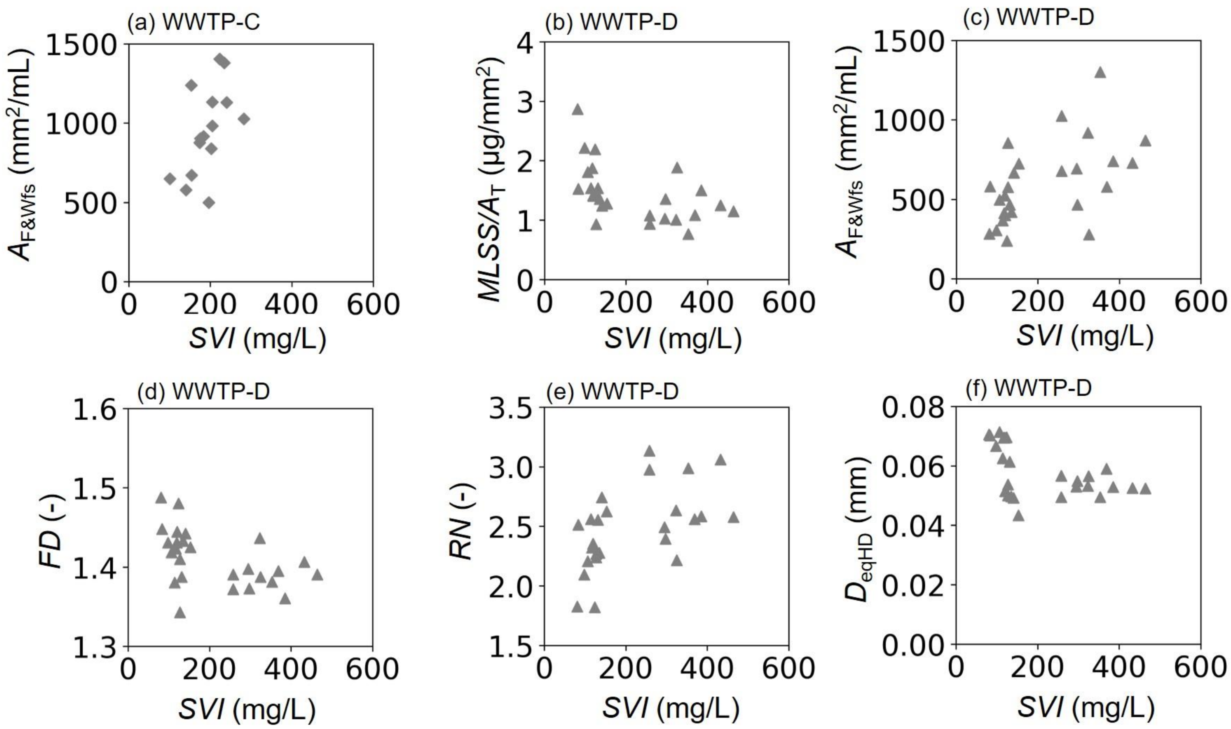


**Fig. 5.** Representative correlation diagrams between *SVI* and AS parameters: (a) *SVI* versus the $A_{F\&Wfs}$ of WWTP-C; (b) *SVI* versus the $MLSS/A_T$ of WWTP-D; (c) *SVI* versus the $A_{F\&Wfs}$ of WWTP-D; (d) *SVI* versus the *FD* of WWTP-D; (e) *SVI* versus the *RN* of WWTP-D; (f) *SVI* versus the $D_{eqHD}$ of WWTP-D.

## 4. Discussion

### *4.1 Morphological parameters*

The values of *SVI* of WWTP-C increased in winter and was positively correlated with $A_{F\&Wfs}$ [Figs. 4 and 5(a)]. In WWTP-D, where a larger seasonal variation of *SVI* was observed, *SVI* increased in winter and remained at a high level until spring, and was positively correlated with $A_{F\&Wfs}$ [Figs. 4 and 5(c)], although the correlation coefficient was smaller than that for WWTP-C (Table 2). Since deterioration of settleability due to an increase in filamentous bacteria with a decrease in water temperature has been reported in the previous studies [28,29], the increase in *SVI* of WWTP-C and WWTP-D may also be related to the increase of such bacteria. In the previous study [29], bacterial cells were stained by Neisser staining and unstained debris was removed by image processing. However, in our study, the total areas of filamentous material and fine floc were obtained together without staining. Therefore, the number of filamentous bacteria may not be accurately estimated as much as the contribution of fine floc, and this needs to be considered as a future issue.

In this study, the size, density, and smoothness of AS flocs of WWTP-C exhibited a correlation to dewaterability, and those of WWTP-D were correlated to settleability. Among the specific parameters regarding the three characteristics, the floc size parameter of $D_{eqHD}$ was correlated to dewaterability in WWTP-C [Fig. 3(e), Table 2] and settleability in WWTP-D [Fig. 5(f), Table 2]. Similarly, $MLSS/A_T$ (density) was correlated to dewaterability in WWTP-C [Fig. 3(b)] and settleability in WWTP-D [Fig. 5(a), Table 2]. Although $A_{HD}/A_T$ was also considered to be one of the parameters related to density, it exhibited a correlation only to dewaterability in WWTP-C [Fig. 3(c), Table 2]. Even though the smoothness of the floc was considered to affect settleability according to previous studies [28,30], the specific parameters of smoothness ($A_{F\&Wfs}$, *FD*, and *RN*) mostly exhibited a small correlation to dewaterability in WWTP-C ($|\text{correlation coefficient}| < 0.60$) (Table 2). As a result, $D_{eqHD}$ and $MLSS/A_T$ can be possible parameters that can commonly explain dewaterability and settleability. Hence, the use of these parameters to control and predict dewaterability and settleability is suggested.

As $MLSS/A_T$ and $D_{eqHD}$ directly describe the floc size and density, respectively, sludge settleability increased with the increase in these parameters [Figs. 5(a) and (f)] [4]. In addition, because the decrease in the AS density might be related to the trapping of a large amount of interstitial water molecules between AS flocs [31,32], the dewatering of low-density ($MLSS/A_T$) AS was considered to be difficult in this study [Fig. 3(b)], as discussed in previous studies [32].

On the other hand, the floc size was considered to not be a sole or a direct parameter of dewaterability, because not only floc size but also several characteristics (e.g., floc strength and structure, surface charge density, and organic content, etc.) were considered to be important for dewaterability, as suggested in previous studies [3,31,32]. Nevertheless, to the best of our knowledge, large flocs tend to exhibit good dewaterability. For example, Yousefi et al. reported that the dewaterability of larger flocs was better than that of smaller flocs with narrow capillaries because these flocs did not release water easily [33]. In another previous study, the size of the sludge conditioned by $Fe^{2+}/Ca(ClO)_2$ was greater than that conditioned by $Fe^{2+}/H_2O_2$, and the sludge pretreatment by $Fe^{2+}/Ca(ClO)_2$ could achieve a deep dewatering performance [34]. These indications were consistent with our results that $D_{eqHD}$ was positively correlated to dewaterability [Fig. 3(e)]. However, the other parameters for size (e.g., $A_T$, $A_{HD}$, $Radius_{max}$) except for $D_{eqHD}$ did not exhibit a significant correlation to dewaterability (Table 2). Notably, $D_{eqHD}$ was related to the size in terms of its definition, but it was not the actual diameter, which cannot be calculated due to the complicated shape. Therefore, $D_{eqHD}$ can be considered as a comprehensive parameter including multiple morphological characteristics of AS, which were not included in the other direct parameters of size (e.g., $A_T$, $A_{HD}$, $Radius_{max}$).

### *4.2 EPS*

The deterioration of sludge settleability was observed in WWTP-B, WWTP-C, and WWTP-D at low water temperatures (Fig. 4, Fig. S1). With the decrease in the temperature, the viscosity of water is well known to increase, which deteriorates sludge settling [35,36]. Poor settleability also might be caused by the release of a high content of EPS from flocs at low temperatures, resulting in the weaker binding strength of EPS between microbial cells [37]. The decrease in lipid solubility at low temperatures can cause specific hydrophobic microorganisms to outcompete other lipid-utilizing microorganisms [36]. Despite these previous studies, our results suggested no significant correlation between the EPS and the actual settleability of AS (Table 2). This result implied that not only determining EPS but combining image analysis is more beneficial for analyzing dewaterability and settleability.

*4.3 Implications*

As one of the cost-effective daily inspection methods for AS, morphology analysis was conducted in this study, as well as deep-learning-based analysis in a previous study [21], which utilized AS floc images obtained by an inexpensive zoom scope. In particular, in this study, no more than 20 min was spent on the preparation of the glass slides to obtaining the final floc morphology for one sample. On the other hand, EPSs were also found to affect the deterioration of dewaterability in WWTP-C. However, as the extraction and evaluation of EPS required considerably more equipment, as well as incurred more labor and time, in comparison with those required for filtration and settlement tests, which also incurred labor and time, the use of image analyses for the rapid diagnosis and prediction of changes in dewaterability and settleability as actual AS behaviors was suggested. To render image analysis as a technology for practical applications to a treatment plant, the relationship between information obtained from an AS image and treatment performance must be investigated.

Notably, in this study, a high-precision motorized XY stage was employed to capture all of the AS flocs on the slide. Equipment cost of the stage can possibly be reduced by the introduction of image stitching technologies [38,39], which can possibly generate one stitched image with no overlap of floc information from a time-lapse movie or multiple images with marginal overlaps, capturing all of the AS flocs on a slide by moving a manual stage. In the future, additional research and improvement as described above will be conducted.

## 5. Conclusions

Dewatering and settling characteristics of AS in four WWTPs were evaluated by their representative parameters, *TTF* and *SVI*, respectively. Among the investigated WWTPs, *TTF* and *SVI* exhibited considerable variations during the 1-year monitoring period, even though the WWTPs were servicing the same city. By using the image analysis setup including the commercial digital microscope, the automated XY stage, and software, morphological parameters were obtained within 20 min, possibly with equipment costs less than those using a commercial optical microscope equipped with a camera. Then, the relationship between the shape/EPS characteristics and dewaterability/settleability values was evaluated especially for WWTP-C and WWTP-D, which exhibited seasonal variations of *TTF* and *SVI*. These results implied that large, dense, and smooth flocs contained less EPSs and were beneficial to sludge dewaterability of WWTP-C. In addition, AS of WWTP-D with better settlement suggested large, dense, and smooth morphological characteristics. Several parameters exhibited correlation to AS dewaterability and settleability. Especially, the $D_{\mathrm{eqHD}}$ and $MLSS/A_{\mathrm{T}}$ were commonly suggested as parameters explaining dewaterability in WWTP-C and settleability in WWTP-D. However, a significant correlation was not recognized between the EPS and settleability of AS, implying that the combination of image analysis and EPS determination can be more beneficial. These findings were provided by cost-effective quantified image analysis, which permits the quantification of sludge morphology from daily analyses of a WWTP and provides considerable data for additional detailed analysis.

## Supporting Information

Supplementary Materials contain one table and one figure. The materials are available free of charge via the Internet (https://doi.org/10.1080/09593330.2023.2240026).


## Acknowledgements

We are grateful to the staff of Sapporo City for providing samples and to Mr. Sho Taniuchi of Hokkaido University for technical support with respect to sampling and equipment maintenance. We would like to thank Uni-edit (https://uni-edit.net/) for editing and proofreading this manuscript.

## Funding

This research was supported financially by the JST-Mirai Program (grant number JPMJMI18DB), JSPS KAKENHI (grant numbers 21H04568, 20KK0090, 19K21979, and 17K18894), a Gesuido Academic Incubation to Advanced (GAIA) Project awarded by the Ministry of Land, Infrastructure, Transport and Tourism (MLIT) (grant number 2016-4), the

Northern Advancement Center for Science & Technology (NOASTEC) (grant number 2016-Startup-7), and the Toda Scholarship Foundation (grant number 2016-1).

## Disclosure statement

The authors declare that they have no known competing financial interests or personal relationships that could have appeared to influence the work reported in this paper.

## Data availability statement

The data that support the findings of this study are available on request from the corresponding author, YN. The data are not publicly available because some information on sewage samples requires permission from the city.

## REFERENCES

[1] Kõrgmaa V, Kriipsalu M, Tenno T, et al. Factors affecting SVI in small scale WWTPs. Water Science and Technology [Internet]. 2019;79:1766–1776. Available from: https://iwaponline.com/wst/article/79/9/1766/67631/Factors-affecting-SVI-in-small-scale-WWTPs.

[2] Guo J, Peng Y, Wang S, et al. Filamentous and non-filamentous bulking of activated sludge encountered under nutrients limitation or deficiency conditions. Chemical Engineering Journal [Internet]. 2014;255:453–461. Available from: https://linkinghub.elsevier.com/retrieve/pii/S1385894714008067.

[3] Christensen ML, Keiding K, Nielsen PH, et al. Dewatering in biological wastewater treatment: A review. Water Research [Internet]. 2015;82:14–24. Available from: https://linkinghub.elsevier.com/retrieve/pii/S0043135415002481.

[4] Tansel B. Morphology, composition and aggregation mechanisms of soft bioflocs in marine snow and activated sludge: A comparative review. Journal of Environmental Management [Internet]. 2018;205:231–243. Available from: https://doi.org/10.1016/j.jenvman.2017.09.082.

[5] Sheng GP, Yu HQ, Li XY. Extracellular polymeric substances (EPS) of microbial aggregates in biological wastewater treatment systems: A review [Internet]. Biotechnology Advances. 2010. p. 882–894. Available from: https://linkinghub.elsevier.com/retrieve/pii/S0734975010001035.

[6] Zhang W, Peng S, Xiao P, et al. Understanding the evolution of stratified extracellular polymeric substances in full-scale activated sludges in relation to dewaterability. RSC Advances [Internet]. 2015;5:1282–1294. Available from: http://xlink.rsc.org/?DOI=C4RA13379J.

[7] Wilén B-M, Lumley D, Mattsson A, et al. Relationship between floc composition and flocculation and settling properties studied at a full scale activated sludge plant. Water Research [Internet]. 2008;42:4404–4418. Available from: https://linkinghub.elsevier.com/retrieve/pii/S0043135408003096.

[8] Shen Y, Huang D-M, Chen Y-P, et al. New insight into filamentous sludge bulking during wastewater treatment: Surface characteristics and thermodynamics. Science of The Total Environment [Internet]. 2020;712:135795. Available from: https://linkinghub.elsevier.com/retrieve/pii/S0048969719357900.

[9] Peng G, Ye F, Li Y. Investigation of extracellular polymer substances (EPS) and physicochemical properties of activated sludge from different municipal and industrial wastewater treatment plants. Environmental Technology [Internet]. 2012;33:857–863. Available from: http://www.tandfonline.com/doi/abs/10.1080/09593330.2011.601763.

[10] Cetin S, Erdincler A. The role of carbohydrate and protein parts of extracellular polymeric substances on the dewaterability of biological sludges. Water Science and Technology [Internet]. 2004;50:49–56. Available from: https://iwaponline.com/wst/article/50/9/49/11042/The-role-of-carbohydrate-and-protein-parts-of.

[11] Li XY, Yang SF. Influence of loosely bound extracellular polymeric substances (EPS) on the flocculation, sedimentation and dewaterability of activated sludge. Water Research [Internet]. 2007;41:1022–1030. Available from: https://linkinghub.elsevier.com/retrieve/pii/S0043135406003976.

[12] Hong C, Si Y, Xing Y, et al. Effect of surfactant on bound water content and extracellular polymers substances distribution in sludge. RSC Advances [Internet]. 2015;5:23383–23390. Available from: http://xlink.rsc.org/?DOI=C4RA15370G.

[13] Li ZH, Han D, Yang CJ, et al. Probing operational conditions of mixing and oxygen deficiency using HSV color space. Journal of Environmental Management. 2019;232:985–992.

[14] Yu Z, Hu Y, Dzakpasu M, et al. Dynamic membrane bioreactor performance enhancement by powdered activated carbon addition: Evaluation of sludge morphological, aggregative and microbial properties. Journal of Environmental Sciences (China) [Internet]. 2019;75:73–83. Available from: https://doi.org/10.1016/j.jes.2018.03.003.

[15] Jin B, Wilén B-M, Lant P. Impacts of morphological, physical and chemical properties of sludge flocs on dewaterability of activated sludge. Chemical Engineering Journal [Internet]. 2004;98:115–126. Available from: https://linkinghub.elsevier.com/retrieve/pii/S1385894703002183.

[16] Van Dierdonck J, Van den Broeck R, Vansant A, et al. Microscopic Image Analysis versus Sludge Volume Index to Monitor Activated Sludge Bioflocculation: A Case Study. Separation Science and Technology [Internet]. 2013;48:1433–1441. Available from: http://www.tandfonline.com/doi/abs/10.1080/01496395.2013.767836.

[17] Koivuranta E, Keskitalo J, Haapala A, et al. Optical monitoring of activated sludge flocs in bulking and non-bulking conditions. Environmental Technology [Internet]. 2013;34:679–686. Available from: http://www.tandfonline.com/doi/abs/10.1080/09593330.2012.710410.

[18] Li Z-H, Guo Y, Hang Z-Y, et al. Simultaneous evaluation of bioactivity and settleability of activated sludge using fractal dimension as an intermediate variable. Water Research [Internet]. 2020;178:115834. Available from: https://doi.org/10.1016/j.watres.2020.115834.

[19] Kuśnierz M. Scale of Small Particle Population in Activated Sludge Flocs. Water, Air, & Soil Pollution [Internet]. 2018;229:327. Available from: http://link.springer.com/10.1007/s11270-018-3979-7.

[20] Chen Q, Wang Y. Influence of single- and dual-flocculant conditioning on the geometric morphology and internal structure of activated sludge. Powder Technology [Internet]. 2015;270:1–9. Available from: http://dx.doi.org/10.1016/j.powtec.2014.10.002.

[21] Satoh H, Kashimoto Y, Takahashi N, et al. Deep learning-based morphology classification of activated sludge flocs in wastewater treatment plants. Environmental Science: Water Research and Technology. 2021;7:298–305.

[22] Satoh H, Kikuchi K, Katayose Y, et al. Simple and reliable enumeration of Escherichia coli concentrations in wastewater samples by measuring β-d-glucuronidase (GUS) activities via a microplate reader. Science of The Total Environment [Internet]. 2020;715:136928. Available from: https://www.sciencedirect.com/science/article/pii/S0048969720304381.

[23] Baird RB, Eaton AD. Standard Methods for the Examination of Water and Wastewater, 23st ed. American Water Works Association/American Public Works Association/Water Environment Federation. Washington DC, USA; 2017.

[24] Frølund B, Palmgren R, Keiding K, et al. Extraction of extracellular polymers from activated sludge using a cation exchange resin. Water Research. 1996;30:1749–1758.

[25] Grijspeerdt K, Verstraete W. Image analysis to estimate the settleability and concentration of activated sludge. Water Research. 1997;31:1126–1134.

[26] Tian Y, Chen L, Zhang S, et al. Correlating membrane fouling with sludge characteristics in membrane bioreactors: An especial interest in EPS and sludge morphology. Bioresource Technology. 2011;102:8820–8827.

[27] Mesquita DP, Amaral AL, Ferreira EC. Identifying different types of bulking in an activated sludge system through quantitative image analysis. Chemosphere [Internet]. 2011;85:643–652. Available from: http://dx.doi.org/10.1016/j.chemosphere.2011.07.012.

[28] Campbell K, Wang J, Daniels M. Assessing activated sludge morphology and oxygen transfer performance using image analysis. Chemosphere. 2019;223:694–703.

[29] Liwarska-Bizukojc E, Andrzejczak O, Solecka M. Study on activated sludge flocs morphology and composition in a full-scale wastewater treatment plant in Poland. Environment Protection Engineering [Internet]. 2019;45:69–82. Available from: http://dx.doi.org/10.37190/epe190205.

[30] Burger W, Krysiak-Baltyn K, Scales PJ, et al. The influence of protruding filamentous bacteria on floc stability and solid–liquid separation in the activated sludge process. Water Research. 2017;123:578–585.

[31] Yousefi SA, Nasser MS, Hussein IA, et al. Influence of polyelectrolyte architecture on the electrokinetics and dewaterability of industrial membrane bioreactor activated sludge. Journal of Environmental Management. 2019;233:410–416.

[32] Wang HF, Hu H, Wang HJ, et al. Comprehensive investigation of the relationship between organic content and waste activated sludge dewaterability. Journal of Hazardous Materials [Internet]. 2020;394:122547. Available from: https://doi.org/10.1016/j.jhazmat.2020.122547.

[33] Yousefi SA, Nasser MS, Hussein IA, et al. Enhancement of flocculation and dewaterability of a highly stable activated sludge using a hybrid system of organic coagulants and polyelectrolytes. Journal of Water Process Engineering. 2020;35.

[34] Yu W, Wen Q, Yang J, et al. Unraveling oxidation behaviors for intracellular and extracellular from different oxidants (HOCl vs. H2O2) catalyzed by ferrous iron in waste activated sludge dewatering. Water Research [Internet]. 2019;148:60–69. Available from: https://doi.org/10.1016/j.watres.2018.10.033.

[35] Cardete MA, Mata-Álvarez J, Dosta J, et al. Effect of the mixed liquor parameters on sludge settling for a petrochemical activated sludge system including an aerobic selector.

Journal of Environmental Chemical Engineering [Internet]. 2018;6:1062–1071. Available from: https://doi.org/10.1016/j.jece.2018.01.025.

[36] Deepnarain N, Nasr M, Kumari S, et al. Decision tree for identification and prediction of filamentous bulking at full-scale activated sludge wastewater treatment plant. Process Safety and Environmental Protection [Internet]. 2019;126:25–34. Available from: https://doi.org/10.1016/j.psep.2019.02.023.

[37] Zhang W, Yang P, Xiao P, et al. Dynamic variation in physicochemical properties of activated sludge floc from different WWTPs and its influence on sludge dewaterability and settleability. Colloids and Surfaces A: Physicochemical and Engineering Aspects. 2015;467:124–134.

[38] Chow SK, Hakozaki H, Price DL, et al. Automated microscopy system for mosaic acquisition and processing. Journal of Microscopy [Internet]. 2006;222:76–84. Available from: https://onlinelibrary.wiley.com/doi/10.1111/j.1365-2818.2006.01577.x.

[39] Chalfoun J, Majurski M, Blattner T, et al. MIST: Accurate and Scalable Microscopy Image Stitching Tool with Stage Modeling and Error Minimization. Scientific Reports [Internet]. 2017;7:4988. Available from: http://www.nature.com/articles/s41598-017-04567-y.